Polymer Degradation and Stability 94 (2009) 566–574

Contents lists available at ScienceDirect

Polymer Degradation and Stability

journal homepage: www.elsevier.com/locate/polydegstab

Mathematical modeling of the catalytic degradation of polystyrene in the presence of aluminum chloride

Ioana A. Gianoglio Pantano, Mónica F. Díaz, Adriana Brandolin, Claudia Sarmoria*

Planta Piloto de Ingeniería Química, PLAPIQUI (UNS-CONICET), Camino La Carrindanga km 7, 8000 Bahía Blanca, Buenos Aires, Argentina

ARTICLE INFO

Article history:
Received 21 October 2008
Received in revised form
23 December 2008
Accepted 19 January 2009
Available online 23 February 2009

Keywords:
Mathematical modeling
Polystyrene degradation
Lewis acid
Molecular weight
Kinetics

ABSTRACT

We model the effect of the catalyst $AlCl_3$ on polystyrene (PS). Detailed experimental studies were previously carried out on the effect of $AlCl_3$ on PS, as part of an effort to understand how to minimize the degradation of PS during the Friedel–Crafts alkylation performed to obtain a graft copolymer from immiscible blends of PS and a polyolefin (PO). In the present work three mathematical models for the catalytic degradation of PS are proposed, all of which consider that reaction starts with the elimination of a phenyl group from the PS chain, followed by either chain scission or a change in the chain structure. The models vary in the way they consider the strength of the main chain bonds, or the reactivity of modified PS chains. Kinetic parameters for each model are estimated. Although the three proposed models could be used to represent our own experimental data, one is more accurate. Experimental data from other authors are used to evaluate its capabilities. Based on the predictions of the better model, we discuss conditions to minimize PS scission, such as operating at low temperatures and $AlCl_3$ concentrations, and using short processing times.

1. Introduction

The disposal of waste plastics has become a critical worldwide problem. That is why the development of recycling techniques has generated great interest in terms of both environmental solution and resource recovery. Moreover, recycling contributes to saving non-renewable raw material consumed in the production of plastics.

The plastics waste stream is composed mainly of commodity thermoplastics such as polyolefins, polystyrene, and polyvinylchloride. These polymers can be recycled by several methods, such as reprocessing, chemical conversion, or incineration with energy recovery among others. In order to avoid the costs associated to the separation of the waste stream into its components, there is great interest in developing processes applicable to mixtures of polymers. Since the polymer species that coexist in the plastic waste are generally immiscible, straightforward blending is impractical. Any attempt at mixing in the molten state results in phase separation, which in turn leads to poor mechanical properties of the solidified blend. In this context, it is necessary to consider compatibilization. This is a useful technique to obtain a synergetic combination of polymer properties [1]. It can be achieved by many methods, but is mostly promoted through copolymers capable of interacting with the different polymer phases. The compatibilizer can be added to the polymer blend or generated in situ through a suitable chemical reaction [2,3]. The latter would be an example of recycling through chemical conversion.

In the case of polystyrene (PS) and polyolefins (POs), two very common components of household waste streams, it is possible to produce a PS-g-PO copolymer using a Friedel–Crafts alkylation reaction [1,4–6]. This reaction is catalyzed by a Lewis acid such as aluminum chloride ($AlCl_3$) and a cocatalyst. Although several kinetic mechanisms have been proposed, the process is not yet completely understood. Under the usual reaction conditions PS degradation due to chain scission has been reported to occur together with the alkylation reaction [7–10]. This undesirable secondary reaction competes with the main copolymerization reaction, degrading the PS and worsening the properties of the PS/PO blend. Since the alkylation takes place at high temperatures ($\approx$200 °C), one should consider that the observed scission may be due to both thermal and catalytic mechanisms.

Both thermal and catalyzed degradation of PS have been widely studied and reported in the literature. Thermal degradation has received more attention [11–17]. Regarding that process, several authors [11–14,20] have proposed the presence of weak links in PS, randomly distributed along the polymer chain, associated with abnormal structures created during polymerization. The existence of weak links was confirmed by Chiantore et al. [11] and Madras et al. [13].

* Corresponding author. Tel.: +54 291 4861700; fax: +54 291 4861600.
E-mail address: csarmoria@plapiqui.edu.ar (C. Sarmoria).

0141-3910/$ – see front matter © 2009 Elsevier Ltd. All rights reserved.
doi:10.1016/j.polymdegradstab.2009.01.015

Under various experimental conditions they observed that the degradation of PS takes place in two distinct stages, one much faster than the other one. The experimental evidence collected by these authors indicates that the fraction of weak bonds in PS is relatively small. The exact nature of these bonds is not completely understood [11]. From the point of view of degradation studies, their main feature is that they are thermally labile. Catalytic degradation has also received attention. A wide range of catalysts that promote degradation have been investigated. In the case of acid catalysts, the ones relevant to the process we study in this work, several kinetic mechanisms as well as mathematical models have been proposed [7–10,18–21]. Some authors have reported crosslinking of polystyrene in the presence of an acid catalyst [10,18], while others have discarded the reaction as negligible [7]. Many of these works were analyzed by Broadbelt [22] in a review of catalytic resource recovery from waste polymers such as polyethylene, polypropylene and PS.

Pukánszky et al. [8] studied the catalytic effect of strong Lewis acids on PS melts, reporting an evident molecular weight decrease. They postulated a mechanism for this chain scission that involved hydride abstraction in the polymer chain by the action of the Lewis acid and the β cleavage of the resulting benzyl cation. Their reaction mechanism was used afterwards by Karmore and Madras [9], who investigated the degradation of PS by Lewis acids in solution. They developed a mathematical model for the number-average molecular weight that explained their experimental observations.

Another reaction mechanism was proposed by Nanbu et al. [10] for the bulk degradation of PS in the presence of an excess of $AlCl_3$. In their mechanism the catalyst forms a complex with water in the presence of moisture traces. The halogen atoms in the catalyst exert a strong pull on the oxygen electrons of the water molecules. As a result, the water protons become weakly bonded to the oxygen [23–25], allowing them to interact with a side-chain phenyl group. The elimination of the phenyl group follows, producing a benzene molecule and a polymeric carbonium ion. The latter induces two reactions: scission of the polymer main chain and formation of an indane skeleton (see Fig. 1) due to intramolecular rearrangement. These conclusions were supported by IR and ^{1}H NMR data analyses [10]. Formation of indane skeletons was also reported in several works that dealt with catalytic degradation of PS in the presence of other acid catalysts [19–21]. Both the degraded PS and the volatile products generated during the process were analyzed. These works reported detection of indane derivatives in the volatile products by GC–MS, and determination of the presence of indane structures in the degraded PS by means of NMR. Theoretical studies of interactions between $AlCl_3$ and aromatic rings suggested that Lewis acids not only generate an electrophile but also have an important role in the activation of the aromatic substrate prior to the electrophile attack [26,27]. This agrees with the mechanism reported by Nanbu et al. [10]. The concentration of $AlCl_3$ does not necessarily remain constant during a modification treatment, as it has been reported that at typical processing conditions this Lewis acid decomposes, even in non-aqueous media [28,29].

Our long-term goal is developing an experimentally validated model of the compatibilization of PS and POs using the Friedel–Crafts reaction in the presence of $AlCl_3$. Industrially, or at technological scale, such a reaction would be carried out in bulk in order to avoid the use of solvents. For this reason, in this work we focus on bulk treatments. As a first step in the development of a comprehensive model, we study the effect of the catalyst on each of the components of the polymeric blend. In the present work, we study the simpler process of bulk degradation of PS in the presence of $AlCl_3$. We evaluate different kinetic mechanisms in order to develop an experimentally validated mathematical model of this particular process. First, experimental data obtained in our laboratory are used to evaluate the models proposed by Karmore and Madras [9] and by Nanbu et al. [10]. We find that the first one is inappropriate for our data. Using the second one as a starting point, we propose three mathematical models of increasing accuracy. Model I considers chain combination, catalyst decomposition, elimination of phenyl groups followed by random chain scission and formation of an indane skeleton in the polymer chain. Model II, besides the above reactions, assumes that the formation of an indane group in the polymer chain results in a less reactive chain. Model III adds to Model I the assumption of different scission rates for the "weak" and "normal" links. For each model, the moment technique is applied to simplify the mass balance equations and facilitate the estimation of the kinetic rate constants.

One of the models is selected, and its capabilities are tested using experimental data reported in the literature by Pukánszky et al. [8] as well as Karmore and Madras [9].

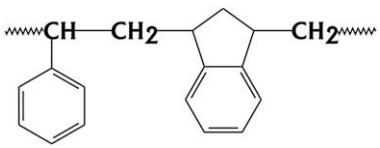

Fig. 1. Indane skeleton.

2. Mathematical models

2.1. Mathematical Model I

2.1.1. Kinetic mechanism I

For this simplified mechanism the following global reactions are considered:

Elimination of phenyl group followed by random chain scission

$$P(x) + A \xrightarrow{k_1} P(x-y-1) + P(y) + A + B \quad x = 2, \ldots, \infty \tag{1}$$

Elimination of phenyl group followed by formation of indane skeleton

$$P(x) + A \xrightarrow{k_2} P(x-1) + A + B \quad x = 2, \ldots, \infty \tag{2}$$

Chain combination

$$P(x) + P(y) + A \xrightarrow{k_3} P(x+y) + A \quad x = 1, \ldots, \infty;\ y = 1, \ldots, \infty \tag{3}$$

Catalyst decomposition

$$A \xrightarrow{k_i} Ai \tag{4}$$

In the above equations, $P(x)$ is a polystyrene molecule with x monomeric units, A is an active catalyst molecule, Ai is an inactive catalyst molecule, and B is a benzene molecule.

We assume that each monomer unit is a reactive site, reactions represented by Eqs. (1)–(3) are of first order with respect to the reactive sites, molecules with indane groups are as reactive as molecules without them, and the catalyst decomposes (Eq. (4)) through a first-order reaction [29]. The kinetic rate constant of the scission reaction is defined as a contribution of two terms in order to improve the model sensitivity, $k_1 = k_{11}A^{\alpha} + k_{12}A^{\beta}$. In this equation, α and β are the orders of the reaction with respect to the

concentration of catalyst. Similarly, the formation of an indane skeleton (Eq. (2)) is of order γ with respect to the concentration of catalyst, while chain combination (Eq. (3)) is of order ε.

A batch isothermal operation is considered and constant reaction volume is assumed. The mass balances for reactions represented by Eqs. (1)–(4) are presented in Eqs. (7)–(10). Brackets are omitted when expressing species molar concentration.

Catalyst

$$\frac{dA}{dt} = -k_i A \tag{5}$$

Benzene

$$\frac{dB}{dt} = \left(k_{11}A^{\alpha} + k_{12}A^{\beta}\right)\sum_{x=2}^{\infty} xP(x) + k_2 A^{\gamma}\sum_{x=2}^{\infty} xP(x) \tag{6}$$

PS molecules with x monomer units (x = 1,…, ∞)

$$\begin{aligned}\frac{dP(x)}{dt} = {} & \left(k_{11}A^{\alpha}+k_{12}A^{\beta}\right)\left[-xP(x)\left(1-\delta_{x,1}\right)\right. \\ & \left.+2\sum_{y=x+1}^{\infty}\Omega(x,y)yP(y)\right]+k_2A^{\gamma}\left[-xP(x)\left(1-\delta_{x,1}\right)\right. \\ & \left.+(x+1)P(x+1)\right]+k_3A^{\varepsilon}\left[-xP(x)\sum_{y=1}^{\infty}yP(y)\right. \\ & \left.+\frac{1}{2}\sum_{y=1}^{x-1}y(x-y)P(y)P(x-y)\left(1-\delta_{x,1}\right)\right]\end{aligned} \tag{7}$$

where $\Omega(x,y)$ determines the distribution of scission products and is given by $1/y$ for random scission [30]. The difference in molar mass between benzene and styrene is neglected.

The above mass balance equations are infinite in number. Then, the well-established moment technique is used to calculate average properties. For that purpose, moment definitions are applied to the polymer length.

The ath-order moment for PS length distribution is defined by

$$M_a = \sum_{x=1}^{\infty} x^a P(x) \tag{8}$$

Experimental data consist of number- and weight-average molecular weights. Therefore, to calculate them it is necessary to obtain expressions for the zeroth, first- and second-order moments.

In order to transform the mass balance shown in Eq. (7), all terms in that equation are multiplied by x^a and then added up for all polymer lengths. Eq. (6) can also be rearranged as a function of the zeroth and first-order moments, since their definitions appear directly in those balances.

Benzene

$$\frac{dB}{dt} = \left(k_{11}A^{\alpha} + k_{12}A^{\beta}\right)(M_1 - P(1)) + k_2A^{\gamma}(M_1 - P(1)) \tag{9}$$

0th-order moment

$$\frac{dM_0}{dt} = \left(k_{11}A^{\alpha}+k_{12}A^{\beta}\right)(M_1+P(1))+k_2A^{\gamma}P(1)-k_3A^{\varepsilon}\frac{M_1^2}{2} \tag{10}$$

1st-order moment

$$\frac{dM_1}{dt} = -\left(k_{11}A^{\alpha}+k_{12}A^{\beta}\right)(M_1-P(1))-k_2A^{\gamma}(M_1-P(1)) \tag{11}$$

2nd-order moment

$$\begin{aligned}\frac{dM_2}{dt} = {} & \left(k_{11}A^{\alpha}+k_{12}A^{\beta}\right)\left(-\frac{M_3}{3}-M_2+\frac{M_1}{3}+P(1)\right) \\ & +k_2A^{\gamma}(M_1-2M_2+P(1))+k_3A^{\varepsilon}M_2^2\end{aligned} \tag{12}$$

In the above equations $P(1)$ is a PS molecule where $x = 1$, and is included in the derivations for completeness. However, since its concentration is much smaller than that of the set of all $P(x)$, its value has been neglected in the calculations.

It should be noted that when solving for the 2nd-order moment, the 3rd-order moment appears in the equation. A closure technique was used as an approximation to estimate it [31]. This yields expressions of the higher order moments as functions of the known lower order ones. An approximate solution results if the type of distribution is not known. In this model, the expression corresponding to a log-normal distribution is used (Eq. (13)).

$$M_3 = M_0\left(\frac{M_2}{M_1}\right)^3 \tag{13}$$

The following measurable quantities may be calculated from the resulting moments.

Number-average molecular weight

$$M_n = 104\,\frac{M_1}{M_0} \tag{14}$$

Weight-average molecular weight

$$M_w = 104\,\frac{M_2}{M_1} \tag{15}$$

As input data the model requires the mass of PS together with its initial number (M_n) and weight (M_w) average molecular weights, mass of catalyst, operating temperature and residence time. Parameter values, such as kinetic rate constants and the exponents α, β, γ and ε, were estimated by fitting the model to experimental information.

2.2. Mathematical Model II

2.2.1. Kinetic mechanism II

In order to evaluate whether indane groups are as reactive as phenyl groups in scission and/or combination reactions, a mathematical model considering that indane groups are less reactive was proposed. Then, PS molecules are allowed to react while the number of indane groups on them is lower than an upper limit, TL.

Elimination of phenyl group followed by random chain scission

$$\begin{aligned}& P(x,r) + A \xrightarrow{k_1} P(x-y-1, r-s) + P(y,s) + A + B \\ & \quad x = 2,\ldots,\infty;\ \ r = 0,1,\ldots,\mathrm{TL}-1\end{aligned} \tag{16}$$

Elimination of phenyl group followed by formation of indane skeleton

$$P(x,r)+A \xrightarrow{k_2} P(x-1,r+1)+A+B \quad x=2,\ldots,\infty;\ r=0,\ldots,\mathrm{TL}-1 \tag{17}$$

Elimination of phenyl group followed by chain combination

$$P(x,r)+P(y,s)+A \xrightarrow{k_3} P(x+y-1,r+s+1)+A+B \quad x=1,\ldots,\infty;\ y=1,\ldots,\infty;\ r=0,1,\ldots,\mathrm{TL}-1;\ s=0,1,\ldots,\mathrm{TL}-1. \tag{18}$$

Catalyst decomposition

$$A \xrightarrow{k_i} Ai \tag{19}$$

In the above equations, $P(x,r)$ is a PS molecule with x monomeric units and r indane groups, A is an active catalyst molecule, Ai is an inactive catalyst molecule, and B is a benzene molecule.

TL is assumed to be a fixed value, and is a parameter to be estimated. In what follows, we discriminate the $P(x,r)$ molecules into two types: reactive molecules, $R(x,r)$, with a number of indane groups lower than TL, and non-reactive molecules, $N(x,r)$, with TL or more indane groups.

As before, the kinetic rate constant of the scission reaction is defined as a contribution of two terms in order to improve the model sensitivity. In particular, this kinetic rate constant is defined as $k_1 = k_{11}A^{\alpha} + k_{12}e^{k_e A}$. As in the previous model, the rates of reaction for the formation of an indane skeleton and for chain combination depend on A^{γ} and A^{ε}, respectively.

Catalyst

$$\frac{dA}{dt} = -k_i A \tag{20}$$

Benzene

$$\frac{dB}{dt} = \left(k_{11}A^{\alpha}+k_{12}e^{k_e A}\right)\sum_{x=2}^{\infty}\sum_{r=0}^{\mathrm{TL}-1} xR(x,r) + k_2A^{\gamma}\sum_{x=2}^{\infty}\sum_{r=0}^{\mathrm{TL}-1} xR(x,r) + \frac{k_3A^{\varepsilon}}{2}\sum_{x=1}^{\infty}\sum_{r=0}^{\mathrm{TL}-1} xR(x,r)\sum_{y=1}^{\infty}\sum_{s=0}^{\mathrm{TL}-1} yR(y,s) \tag{21}$$

Reactive PS molecule with x monomer units and r indane groups ($x = 1,\ldots,\infty$; $r = 0,\ldots,TL-1$)

$$\begin{aligned}\frac{dR(x,r)}{dt} = {} & \left(k_{11}A^{\alpha}+k_{12}e^{k_e A}\right)\left\{-xR(x,r)\left(1-\delta_{x,1}\right) + 2\sum_{y=x+1}^{\infty}\sum_{s=r}^{\mathrm{TL}-1}\Omega[(x,r),(y,s)]yR(y,s)\right\} \\ & + k_2A^{\gamma}\left[-xR(x,r)\left(1-\delta_{x,1}\right)+(x+1)R(x+1,r-1)\right] \\ & + k_3A^{\varepsilon}\left[-xR(x,r)\sum_{y=1}^{\infty}\sum_{s=0}^{\mathrm{TL}-1} yR(y,s) + \frac{1}{2}\sum_{y=1}^{x}\sum_{s=0}^{r} y(y-x+1)R(y,s)R(x-y+1,r-s)\right]\end{aligned} \tag{22}$$

Non-reactive PS molecule with x monomer units and r indane groups ($x = 1,\ldots,\infty$; $r \geq TL$)

$$\frac{dN(x,r)}{dt} = k_2A^{\gamma}(x+1)R(x+1,r-1)\delta_{r,\mathrm{TL}} + k_3A^{\varepsilon}\frac{1}{2}\sum_{y=1}^{x}\sum_{s=1}^{r-1} y(y-x+1)R(y,s)R(x-y+1,r-s) \tag{23}$$

As done in Model I, the moment technique is used to reduce the number of mass balance equations. Moment definitions are applied to the polymer length, both for reactive and non-reactive molecules. The ath-order moment for the length distribution of reactive PS molecules is defined by $M_a = \sum_{x=1}^{\infty}\sum_{r=0}^{\mathrm{TL}-1} x^a R(x,r)$ and for the length distribution of non-reactive PS molecules by $L_a = \sum_{x=1}^{\infty}\sum_{r=\mathrm{TL}}^{2\mathrm{TL}-1} x^a R(x,r)$.

In Eqs. (22) and (23) all terms are multiplied by x^a and then added up for all polymer lengths. Eq. (21) can also be rearranged as a function of M_0 and M_1, since their definitions appear directly.

The moment balance was carried out for both types of molecules, considering that a fraction of each molecule is produced for each proposed reaction. The fraction of each kind of molecule is defined as follows:

$$f_{r1} = \frac{\mathrm{TL}-1}{\mathrm{TL}} = 1 - f_{n1} \tag{24}$$

$$f_{r2} = \frac{\mathrm{TL}-1}{2\mathrm{TL}} = 1 - f_{n2} \tag{25}$$

where f_{r1} and f_{n1} are the fractions of reactive and non-reactive molecules, respectively, produced during the indane skeleton formation reaction. f_{r2} and f_{n2} are the fractions of reactive and non-reactive molecules produced in the chain combination reaction.

Benzene

$$\frac{dB}{dt} = \left(k_{11}A^{\alpha}+k_{12}e^{k_e A}\right)(M_1 - R(1,0)) + k_2A^{\gamma}(M_1 - R(1,0)) + k_3A^{\varepsilon}\frac{M_1^2}{2} \tag{26}$$

0th-order moment

$$\frac{dM_0}{dt} = \left(k_{11}A^{\alpha}+k_{12}e^{k_e A}\right)(M_1 + R(1,0)) - k_2A^{\gamma}\left(\frac{M_1}{\mathrm{TL}} - R(1,0)\right) + k_3A^{\varepsilon}M_1^2\left(\frac{\mathrm{TL}-1}{4\mathrm{TL}} - 1\right) \tag{27}$$

$$\frac{dL_0}{dt} = k_2A^{\gamma}\frac{M_1}{\mathrm{TL}} + k_3A^{\varepsilon}M_1^2\frac{(\mathrm{TL}+1)}{4\mathrm{TL}} \tag{28}$$

1st-order moment

$$\frac{dM_1}{dt} = -\left(k_{11}A^{\alpha}+k_{12}e^{k_e A}\right)(M_1 - R(1,0)) - k_2A^{\gamma}\left(\frac{M_2}{\mathrm{TL}} + M_1\frac{\mathrm{TL}-1}{\mathrm{TL}} - R(1,0)\right) + k_3A^{\varepsilon}\left[-M_1M_2 + \left(M_1M_2 - \frac{M_1^2}{2}\right)\frac{\mathrm{TL}-1}{2\mathrm{TL}}\right] \tag{29}$$

$$\frac{dL_1}{dt} = k_2A^{\gamma}\frac{M_2 - M_1}{\mathrm{TL}} + k_3A^{\varepsilon}\left(M_2M_1 - \frac{M_1^2}{2}\right)\frac{\mathrm{TL}+1}{2\mathrm{TL}} \tag{30}$$

2nd-order moment

$$\frac{dM_2}{dt} = \left(k_{11}A^{\alpha} + k_{12}e^{k_e A}\right)\left(-\frac{M_3}{3} - M_2 + \frac{M_1}{3} + R(1,0)\right) + k_2 A^{\gamma}\left[-M_3 + (M_1 - 2M_2)\frac{TL-1}{TL} + R(1,0)\right] + k_3 A^{\varepsilon}\left[-M_3M_1 + \left(M_3M_1 + M_2^2 - 2M_2M_1 + \frac{M_1^2}{2}\right)\frac{TL-1}{2TL}\right] \quad (31)$$

$$\frac{dL_2}{dt} = k_2 A^{\gamma}\frac{(M_3 - 2M_2 + M_1)}{TL} + k_3 A^{\varepsilon}\left(M_3M_1 + M_2^2 - 2M_2M_1 + \frac{M_1^2}{2}\right)\frac{TL+1}{2TL} \quad (32)$$

In this model $R(1,0)$ is treated in the same way as $P(1)$ in Model I.

The closure relationships corresponding to log-normal distributions are used for both reactive and non-reactive PS molecules. Then, third-order moments are calculated, as explained before, by:

$$M_3 = M_0\left(\frac{M_2}{M_1}\right)^3 \text{ and } L_3 = L_0\left(\frac{L_2}{L_1}\right)^3 \quad (33)$$

Average molecular weights involve both the reactive and the non-reactive molecules.

Number-average molecular weight

$$M_n = 104\,\frac{M_1 + L_1}{M_0 + L_0} \quad (34)$$

Weight-average molecular weight

$$M_w = 104\,\frac{M_2 + L_2}{M_1 + L_1} \quad (35)$$

As input data the model requires the mass of PS, its initial average molecular weights, mass of catalyst, operating temperature and residence time. The model also requires the value of the upper limit of indane groups per PS molecule, TL. This value, together with the parameter values such as kinetic rate constants and the exponents α, ε and γ, was estimated for an accurate fit of the experimental information.

2.3. Mathematical Model III

Experimental data show a rapid decrease in molecular weights at the beginning of the reaction. This fact may be explained by the cleavage of a limited number of weak links present in the PS structure which have a lower activation energy, and therefore a faster scission rate, than the remaining PS normal links [11,13]. Then, the initial number of weak links is considered to be a property of each particular virgin PS polymer, because it depends on the conditions under which it was polymerized. In order to include weak links into the model, Kinetic mechanism I is adopted, but taking into account the difference in bond strength by means of different scission rates for weak and normal links.

The relative number of each kind of link is defined as follows:

$$f_w = \frac{e_w}{e_s + e_w} = \frac{e_w}{\sum_{x=1}^{\infty}(x-1)P(x)} = \frac{e_w}{\sum_{x=1}^{\infty}xP(x) - \sum_{x=1}^{\infty}P(x)} \quad (36)$$

$$f_s = 1 - f_w$$

where f_w is the fraction of weak links and f_s is the fraction of normal links.

Catalyst

$$\frac{dA}{dt} = -k_i A \quad (37)$$

Benzene

$$\frac{dB}{dt} = \left(f_w k_{1w}A^{\alpha} + f_s k_{1s}A^{\beta}\right)\sum_{x=2}^{\infty}xP(x) + k_2 A^{\gamma}\sum_{x=2}^{\infty}xP(x) \quad (38)$$

Weak links

$$\frac{de_w}{dt} = -k_{1w}A^{\alpha}e_w \quad (39)$$

PS molecules with x monomer units ($x = 1,\ldots,\infty$)

$$\frac{dP(x)}{dt} = \left(f_w k_{1w}A^{\alpha} + f_s k_{1s}A^{\beta}\right)\left[-xP(x)(1-\delta_{x,1}) + 2\sum_{y=x+1}^{\infty}Q(x,y)yP(y)\right] + k_2 A^{\gamma}\left[-xP(x)(1-\delta_{x,1}) + (x+1)P(x+1)\right] + k_3 A^{\varepsilon}\left[-xP(x)\sum_{y=1}^{\infty}yP(y) + \frac{1}{2}\sum_{y=1}^{x-1}y(y-x)P(y)P(x-y)(1-\delta_{x,1})\right] \quad (40)$$

Eq. (39) is solved analytically, for a non-zero α coefficient, to obtain e_w, which then is replaced in Eq. (36). The result is:

Fraction of weak links

$$f_w = \frac{\left(e_w(0)e^{\left(k_{1w}\left(A^{\alpha} - A(0)^{\alpha}\right)\right)/\alpha k_i}\right)}{\sum_{x=1}^{\infty}xP(x) - \sum_{x=1}^{\infty}P(x)} \quad (41)$$

As in the previous models, the moment technique is used. Therefore, moments defined in Eq. (8) were applied to Eq. (40). Eqs. (38) and (41) can be also rewritten in terms of moments.

Benzene

$$\frac{dB}{dt} = \left(f_w k_{1w}A^{\alpha} + f_s k_{1s}A^{\beta}\right)(M_1 - P(1)) + k_2 A^{\gamma}(M_1 - P(1)) \quad (42)$$

0th-order moment

$$\frac{dM_0}{dt} = \left(f_w k_{1w}A^{\alpha} + f_s k_{1s}A^{\beta}\right)(M_1 + P(1)) + k_2 A^{\gamma}P(1) - k_3 A^{\varepsilon}\frac{M_1^2}{2} \quad (43)$$

1st-order moment

$$\frac{dM_1}{dt} = -\left(f_w k_{1w} A^{\alpha} + f_s k_{1s} A^{\beta}\right)(M_1 - P(1)) - k_2 A^{\gamma}(M_1 - P(1)) \tag{44}$$

2nd-order moment

$$\frac{dM_2}{dt} = \left(f_w k_{1w} A^{\alpha} + f_s k_{1s} A^{\beta}\right)\left(-\frac{M_3}{3} - M_2 + \frac{M_1}{3} + P(1)\right) + k_2 A^{\gamma}(-2M_2 + M_1 + P(1)) + k_3 A^{\varepsilon} M_2^2 \tag{45}$$

$$f_w = \frac{\left(e_w(0) e^{\left(k_{1w}\left(A^{\alpha} - A(0)^{\alpha}\right)\right)/\alpha k_i}\right)}{M_1 - M_0} \tag{46}$$

As in the previous two models, the value of $P(1)$ was neglected in the calculations.

In this model, a closure relationship corresponding to log-normal weight distribution is also considered. The third-order moment was calculated as expressed in Eq. (13). Average molecular weights were calculated as in Eqs. (14) and (15).

As input data the model requires the mass of PS, its initial average molecular weights, mass of catalyst, operating temperature and residence time. The model also requires the value of the initial number of weak links. This value, together with the remaining parameter values, was estimated by fitting the model to experimental information.

3. Experimental data

In order to validate the models, we used experimental data obtained in our laboratory [7]. Briefly, a molten commercial PS (Lutrex HH-103, Unistar S.A., M_n = 136 000, M_w = 271 000) was treated with 0.1, 0.3, 0.5, 0.7 and 1 wt% of $AlCl_3$. The reaction was performed in a batch mixer at 200 °C and 60 rpm under N_2 atmosphere for 22 min. Samples were withdrawn periodically during mixing. Average molecular weights were analyzed by Size Exclusion Chromatography (SEC) using a Waters Scientific Chromatograph model 150-CV. The solvent used was 1,2,4-trichlorobenzene, with 0.0125 wt% 2,6-di-*tert*-butyl-*p*-cresol added as antioxidant. The injection temperature was 135 °C. Several replications were averaged for each data point, ensuring an error level within the instrument accuracy of ±5%.

The reaction gases collected from the mixer's headspace during blending were analyzed by Gas Chromatography–Mass Spectroscopy (GC–MS) [7]. We used a GC–MS instrument model Clarus 500 (Perkin Elmer). The analytical column connected to the system was a PE-5MS capillary column (60 m × 0.25 mm ID, 0.25 μm film thickness). In the full-scan mode, electron ionization (EI) mass spectra in the range of 35–200 (m/z) were recorded at an electron energy of 70 eV. Compounds were identified with the help of the NIST library, available in the instrument.

The main volatile product formed was benzene, detected at all catalyst concentrations. Other six derivatives of benzene and indane were detected at higher catalyst concentrations: ethylbenzene,

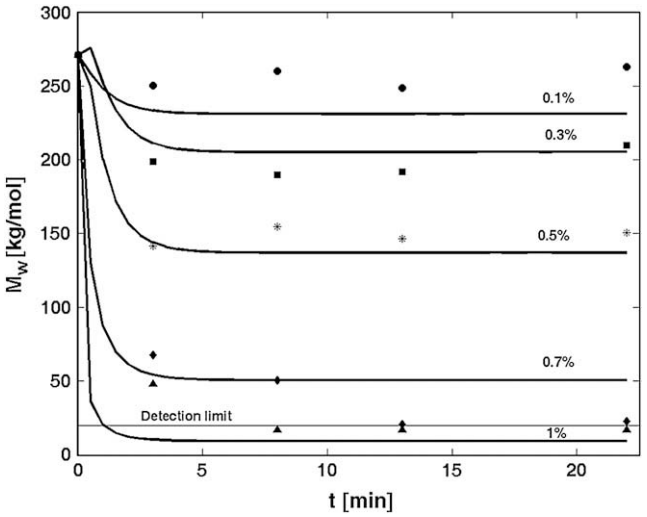

Fig. 3. M_w vs. time at various concentrations of $AlCl_3$. Lines: Model I, symbols: experimental measurements (● 0.1, ■ 0.3, ∗ 0.5, ◆ 0.7, ▲ 1 wt% $AlCl_3$).

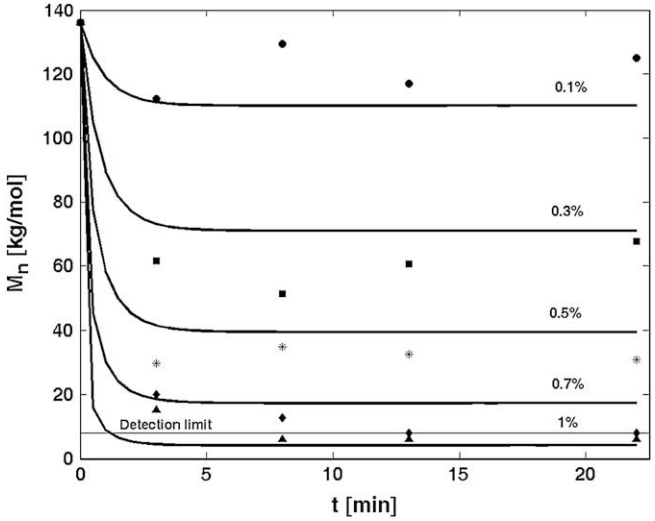

Fig. 2. M_n vs. time at various concentrations of $AlCl_3$. Lines: Model I, symbols: experimental measurements (● 0.1, ■ 0.3, ∗ 0.5, ◆ 0.7, ▲ 1 wt% $AlCl_3$).

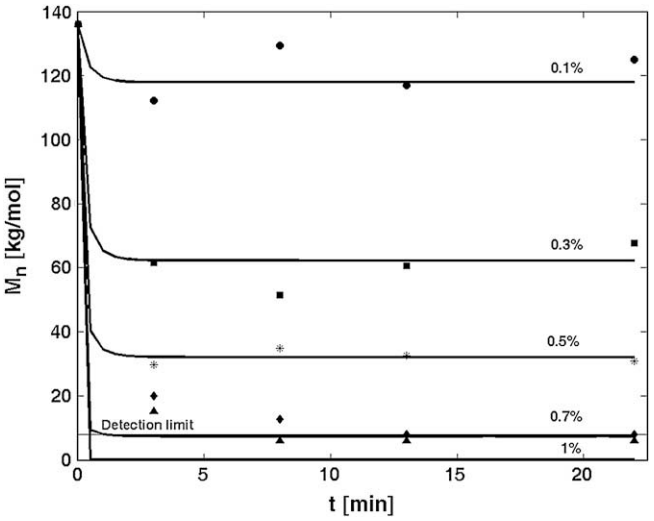

Fig. 4. M_n vs. time at various concentrations of $AlCl_3$. Lines: Model II, symbols: experimental measurements (● 0.1, ■ 0.3, ∗ 0.5, ◆ 0.7, ▲ 1 wt% $AlCl_3$).

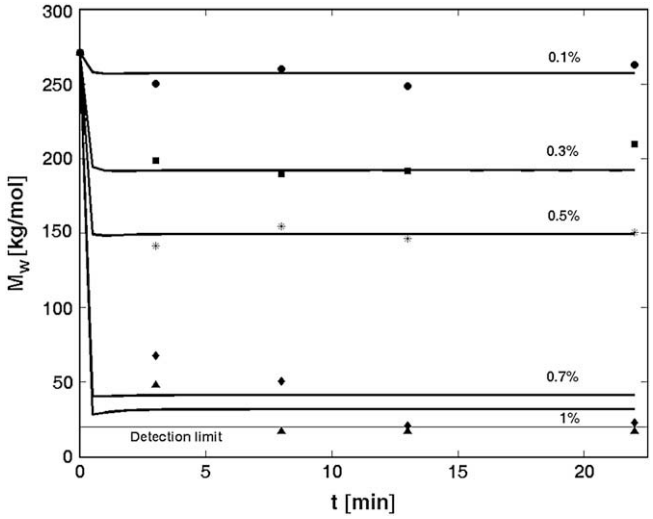

Fig. 5. M_w vs. time at various concentrations of $AlCl_3$. Lines: Model II, symbols: experimental measurements (● 0.1, ■ 0.3, ∗ 0.5, ◆ 0.7, ▲ 1 wt% $AlCl_3$).

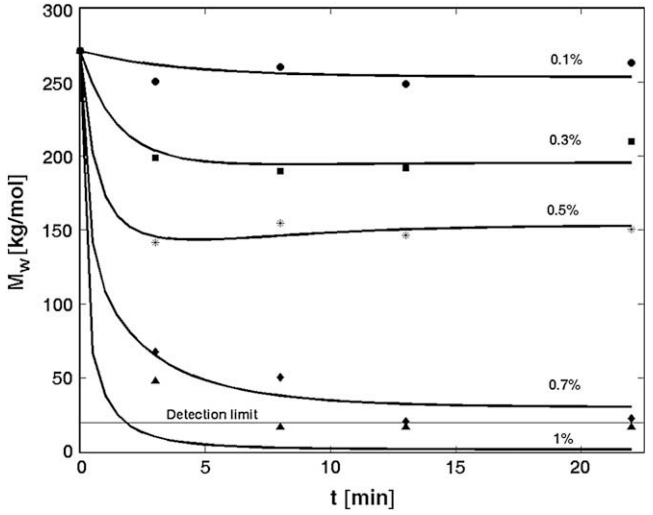

Fig. 7. M_w vs. time at various concentrations of $AlCl_3$. Lines: Model III, symbols: experimental measurements (● 0.1, ■ 0.3, ∗ 0.5, ◆ 0.7, ▲ 1 wt% $AlCl_3$).

ethylmethylbenzene, indane, 1-methyl indane, and two isomers of dimethyl indane. The concentration of every volatile product increased with catalyst concentration. These observations support those proposed kinetic mechanisms that involve elimination of phenyl groups as a starting step, followed by chain scission reactions and the formation of indane groups [10,19–21]. More details on the experiments may be found elsewhere [7].

4. Parameter estimation

The three proposed mathematical models have parameters that need to be estimated, namely the kinetic rate constants and other values such as the initial number of weak links. For this task we used the commercial software gPROMS (generalized PROcess Modelling System) and the experimental data described above.

The parameter estimation was performed by evaluation of the following objective function [32]:

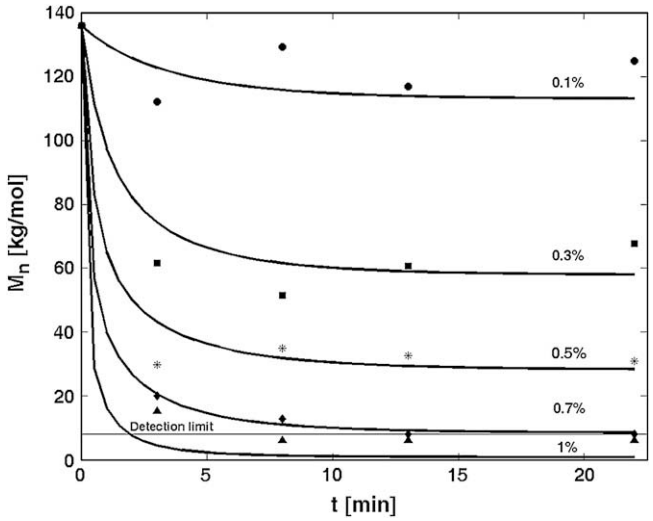

Fig. 6. M_n vs. time at various concentrations of $AlCl_3$. Lines: Model III, symbols: experimental measurements (● 0.1, ■ 0.3, ∗ 0.5, ◆ 0.7, ▲ 1 wt% $AlCl_3$).

$$ObjF = \frac{N}{2}\ln(2\pi) + \frac{1}{2}\min_{\theta}\left\{\sum_{i=1}^{NE}\sum_{j=1}^{NV_i}\sum_{k=1}^{NM_{ij}}\left[\ln\left(\sigma_{ijk}^2\right) + \frac{\left(\tilde{z}_{ijk} - z_{ijk}\right)^2}{\sigma_{ijk}^2}\right]\right\} \quad (47)$$

where N is the total number of measurements, θ is the set of model parameters to be estimated, NE is the number of experiments, NV_i is the number of variables measured in the ith experiment, NM_{ij} is the number of measurements of the jth variable in the ith experiment, σ_{ij}^2 is the variance of the kth measurement of variable j in experiment i, and, $\tilde{z}_{ijk}$ and z_{ijk} are the kth measured and calculated values of variable j in experiment i, respectively. The variance was specified as constant, with different values for different experiments.

5. Results and discussion

The effect of $AlCl_3$ on the degradation of PS was studied by analyzing the change of M_n and M_w with time. This is shown in Figs. 2–7 for catalyst concentrations between 0.1 and 1 wt%. The plots show a rapid initial decrease of molecular weights for all concentrations of catalyst, decrease that is more pronounced for higher concentrations. After this first stage, the molecular weights remain almost constant for the lower concentrations of $AlCl_3$, 0.1–0.5 wt%, while for 0.7 wt% the molecular weights continue decreasing. For 1 wt% of $AlCl_3$ the degradation is so fast that after a few minutes the molecular weights fall below the detection limit

Table 1
Estimated parameters – Model I.

Parameter	Value
k_{11} (scission)	2.27×10^5 M^{-2} min^{-1}
k_{12} (scission)	1.63×10^{14} M^{-4} min^{-1}
k_2 (indane formation)	2.36×10^4 M^{-1} min^{-1}
k_3 (chain combination)	6.141×10^7 M^{-3} min^{-1}
k_i (catalyst decomposition)	1.029 min^{-1}
α (scission)	2
β (scission)	4
γ (indane formation)	1
ε (chain combination)	2

Table 2
Estimated parameters – Model II.

Parameter	Value
k_{11} (scission)	5.40×10^{6} M^{-2} min^{-1}
k_{12} (scission)	4.5951×10^{-9} min^{-1}
k_e (scission)	2.592×10^{5} M^{-1}
k_2 (indane formation)	1.775×10^{3} M^{-1} min^{-1}
k_3 (chain combination)	1.414×10^{3} M^{-2} min^{-1}
k_i (catalyst decomposition)	1.2594 min^{-1}
α (scission)	2
γ (indane formation)	1
ε (chain combination)	1

of the instrument, making the data unreliable for a proper model evaluation.

The resulting parameters for each model are shown in Tables 1–3. For Models I and III, scission rate dependence on the fourth power of the catalyst concentration is in agreement with reported kinetic mechanisms in similar conditions [9]. This high-order coefficient may indicate a complex degradation process. For Model II, the maximum number of indane groups was TL = 24. In the case of Model III the initial concentration of weak links was estimated to be 0.09998 M, which is 1.031×10^{-5} mol weak links/g PS.

Figs. 2 and 3 show the variation of the average molecular weights (M_n and M_w, respectively) with reaction time, both experimental and estimated with Model I. The model predicts the trends of the experimental data. It considers that the scission rate consists of two terms which show different dependence on the catalyst concentration. As indicated in Table 1, one term was estimated to be of second order, representing the effect of low catalyst concentration on molecular weight, and the other term was estimated to be of fourth order, representing the high catalyst concentration effect. However, it is not able to predict the change in the slope of the molecular weight vs. time curves after the initial stage that occurs for the higher concentrations of catalyst. In those cases the experimentally observed molecular weights continue decreasing instead of remaining constant.

Figs. 4 and 5 show experimental and calculated molecular weights as functions of reaction time for Model II. This model fits the experimental data for low concentrations of catalyst (0.1–0.5 wt%). The fast molecular weight stabilization, not displayed by Model I results, may be explained not only by the higher catalyst decomposition rates but also by the assumption of the generation of non-reactive PS molecules. Even though the accuracy is improved with respect to the previous model, Model II is not able to predict the molecular weight decrease when high concentrations of catalyst, 0.7 and 1 wt%, are used. The reason may be that this model predicts that the fast catalyst decomposition stops PS from reacting at long times.

Table 3
Estimated parameters – Model III.

Parameter	Value
k_{1w} (weak link scission)	4.83×10^{8} M^{-2} min^{-1}
k_{1s} (normal link scission)	3.97×10^{13} M^{-4} min^{-1}
k_2 (indane formation)	9.885×10^{7} M^{-2} min^{-1}
k_3 (chain combination)	2.603×10^{7} M^{-3} min^{-1}
k_i (catalyst decomposition)	1.203×10^{-1} min^{-1}
α (weak link scission)	2
β (normal link scission)	4
γ (indane formation)	2
ε (chain combination)	2

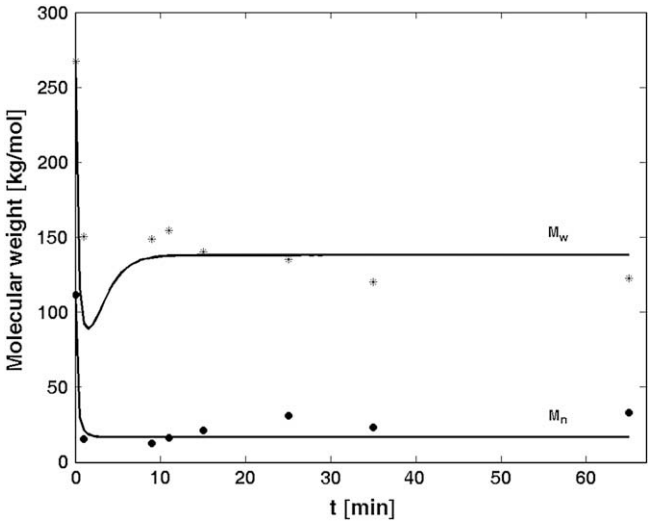

Fig. 8. M_n (●) and M_w (✳) vs. time. Lines: Model III, symbols: experimental measurements from Pukánszky et al. [8].

Model III predictions are shown in Figs. 6 and 7. This model is able to describe the molecular weight behavior in the entire time range: at short reaction times, the decrease in the molecular weight may be explained by the cleavage of weak links. After that, when the catalyst concentrations are low (0.1–0.5 wt%), molecular weight remains constant, due to the opposing effects of the chain combination and scission reactions. When the catalyst concentrations are high (0.7–1 wt%), molecular weight continues to decrease due to the cleavage of the normal links. For catalyst contents of 1 wt% the predicted average molecular weights fall below the instrument detection limit just as the experimental ones do.

In order to evaluate the accuracy of Model III, experimental data from Pukánszky et al. [8] and Karmore and Madras [9] were used. It should be noted that these experiments were carried out at different temperatures and assay conditions. Karmore and Madras [9] worked with PS in solution at 75, 100 and 125 °C, at two different $AlCl_3$ concentrations. In both cases the $AlCl_3$/PS ratio was close to unity. These authors only evaluated the evolution of M_n. On

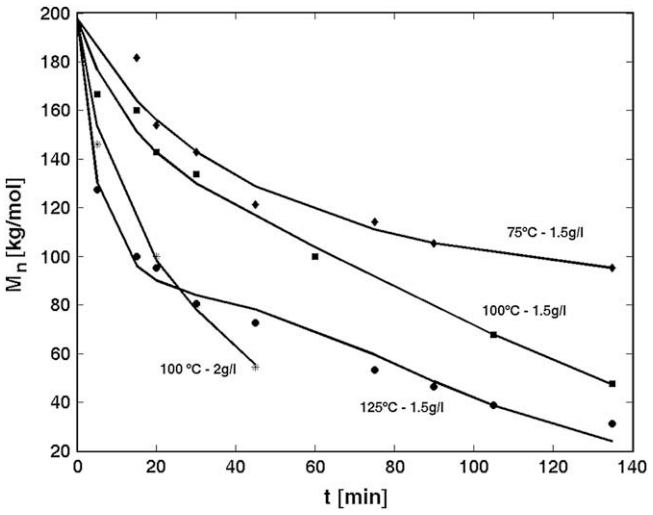

Fig. 9. M_n vs. time at various temperatures and two $AlCl_3$ concentrations. Lines: Model III, symbols: experimental measurements from Karmore and Madras [9] (◆ 75 °C – 1.5 g l^{-1}, ■ 100 °C – 1.5 g l^{-1}, ● 125 °C – 1.5 g l^{-1}, ✳ 100 °C – 2 g l^{-1}).

Table 4
Estimated parameters. Evaluation of Model III.

	Karmore and Madras [9], 75 °C	Karmore and Madras [9], 100 °C	Karmore and Madras [9], 125 °C	Pukánszky et al. [8], 180 °C
k_{1w} (M^{-2} min^{-1})	61.8	302.9	6.65×10^{2}	8.54×10^{6}
k_{1s} (M^{-4} min^{-1})	0	392	1.22×10^{3}	1.44×10^{12}
k_2 (M^{-2} min^{-1})	2.75	102.3	1.12×10^{2}	2.62×10^{6}
k_3 (M^{-3} min^{-1})	2	40.07	56.0	7.104×10^{6}
k_i (min^{-1})	5.69×10^{-14}	9.81×10^{-14}	3.36×10^{-12}	0.3
e_w initial (M)	2.40×10^{-5}	2.40×10^{-5}	2.40×10^{-5}	0.107

the other hand, Pukánszky et al. [8] worked with molten PS at 180 °C. Since the experimental conditions are so different from the ones used in our own experiments, we could not apply the parameters estimated in Section 4. New values for the kinetic rate constants and initial concentration of weak links were estimated for each experimental set, using the reaction orders that we had estimated previously. Results are shown in Figs. 8 and 9 and in Table 4.

Fig. 8 shows a good model fit for the data of Pukánszky et al. [8]. The model shows a minimum in M_w at short times and a subsequent increase to reach a plateau at 10 min. This could be explained by the balance between chain scission and combination reactions at different times. Unfortunately there are not enough experimental M_w measurements to completely validate the model predictions at short times. However, Pukánszky et al. [8] reported torque measurements that show a minimum at short times, consistent with our predictions.

Fig. 9 shows the model predictions for the data of Karmore and Madras [9]. The agreement with experimental measurements is very good. As may be seen, the slopes of the molecular weight curves are not as steep as the ones observed in the experiments reported by Pukánszky et al. [8]. This may be attributed to the fact that the experiments were carried out in solution, avoiding incomplete mixing problems. Even though Karmore and Madras [9] reported many experimental data at various temperatures, the lack of experimental M_w values restricts the importance of this evaluation because M_n may be calculated accurately with a simple model.

In Table 4 we show estimated rate constants. They are consistently increasing with temperature. Estimated initial weak link concentration is similar in all Karmore and Madras [9] experiments.

6. Conclusions

Three mathematical models for the catalytic degradation of PS with $AlCl_3$ as catalyst were developed and compared. Model parameters, such as kinetic rate constants, reaction orders and specific additional constants were estimated for each one.

The three models consider the reactions of chain scission, formation of indane groups, chain combination and catalyst decomposition, with the production of benzene as a by-product. It must be noted that catalyst decomposition and benzene production are consistent with experimental evidence.

Despite being derived from similar kinetic mechanisms, all three mathematical models show an important difference in accuracy. In general, estimated parameters are different in value. At low catalyst concentrations all models show similar acceptable trends. In this concentration range molecular weights decrease only at short reaction times, something that can be explained by the cleavage of weak links present in PS. At high catalyst concentrations, molecular weights continue decreasing after the initial drop. This could only be explained by Model III, because it allows the cleavage of normal, and thus stronger, links. Therefore, Model III was selected as the model that fitted better our experimental data. It was also able to represent satisfactorily experimental data reported in the literature for different reaction conditions [8,9] after performing suitable parameter estimations.

The experimental evidence analyzed in this work indicates that in order to minimize PS decomposition one should operate at low temperatures and $AlCl_3$ concentrations. It is also desirable to avoid long processing times, so as to preserve the normal links from scission. However, when considering the production of PS-g-PO copolymer other considerations will be important, since the optimal conditions for the grafting reaction will not necessarily coincide with those that minimize scission as a stand-alone reaction. It will be necessary to find operating conditions to optimize grafting while minimizing the secondary scission reaction. In order to accomplish this task, a more complete model that includes both the degradation and graft reactions is needed. Work is under way in this direction, using Model III as a starting point.

Acknowledgements

The authors wish to thank CONICET (National Research Council of Argentina), ANPCyT (National Agency for Promotion of Science and Technology of Argentina), and UNS (Universidad Nacional del Sur) for financial support.

References

[1] Díaz MF, Barbosa SE, Capiati NJ. Polymer 2007;48(4):1058–65.
[2] Bisio AL, Xanthos M. How to manage plastics waste: technology and market opportunities. Munich: Hanser; 1995.
[3] Goodship V. Sci Prog 2007;90(4):245–68.
[4] Carrick WL. J Polym Sci Part A Polym Chem 1970;8(1):215–23.
[5] Sun YJ, Baker WE. J Appl Polym Sci 1997;65(7):1385–93.
[6] Díaz MF, Barbosa SE, Capiati NJ. Polymer 2002;43(18):4851–8.
[7] Díaz MF, Barbosa SE, Capiati NJ. J Polym Sci Part A Polym Chem, submitted for publication.
[8] Pukánszky B, Kennedy JP, Kelen T, Tüdõs F. Polym Bull 1981;5(8):469–76.
[9] Karmore V, Madras G. Ind Eng Chem Res 2002;41(2):657–60.
[10] Nanbu H, Sakuma Y, Ishihara Y, Takesue T, Ikemura T. Polym Degrad Stab 1987;19(1):61–76.
[11] Chiantore O, Camino G, Costa L, Grassie N. Polym Degrad Stab 1981;3(3):209–19.
[12] Kishore K, Pai Verneker VR, Nair MNR. J Appl Polym Sci 1976;20(9):2355–65.
[13] Madras G, Smith JM, McCoy BJ. Polym Degrad Stab 1997;58(1–2):131–8.
[14] Madras G, Chung GY, Smith JM, McCoy BJ. Ind Eng Chem Res 1997;36(6):2019–24.
[15] Kruse TM, Woo OS, Wong H-W, Khan SS, Broadbelt LJ. Macromolecules 2002;35(20):7830–44.
[16] Faravelli T, Pinciroli M, Pisano F, Bozzano G, Dente M, Ranzi E. J Anal Appl Pyrolysis 2001;60(1):103–21.
[17] Westerhout RWJ, Waanders J, Kuipers JAM, van Swaaij WPM. Ind Eng Chem Res 1997;36(6):1955–64.
[18] Serrano DP, Aguado J, Escola JM. Appl Catal B 2000;25(2–3):181–9.
[19] Audisio G, Bertini F, Beltrame PL, Carniti P. Polym Degrad Stab 1990;29(2):191–200.
[20] Ide S, Ogawa T, Kuroki T, Ikemura T. J Appl Polym Sci 1984;29(8):2561–71.
[21] Ogawa T, Kuroki T, Ide S, Ikemura T. J Appl Polym Sci 1982;27(3):857–69.
[22] Broadbelt LJ. Catalysis, vol. 14. The Royal Society of Chemistry; 1999 [chapter 4].
[23] Solomons G. Organic chemistry. 5th ed. New York: John Wiley; 1992.
[24] Kennedy JP, Marechal E. Carbocationic polymerization. New York: John Wiley and Sons; 1982.
[25] Munk P. Introduction to macromolecular science. New York: John Wiley and Sons; 1989.
[26] Tarakeshwar P, Lee JY, Kim SK. J Phys Chem A 1998;102(13):2253–5.
[27] Tarakeshwar P, Kim KS. J Phys Chem A 1999;103(45):9116–24.
[28] Černý Z, Macháček J, Fusek J, Čásenský B, Kříž O, Tuck D. Inorg Chim Acta 2000;300–302:556–64.
[29] Chattopadhyay S, Madras G. Polym Degrad Stab 2001;73(1):83–6.
[30] McCoy BJ, Wang M. Chem Eng Sci 1994;49(22):3773–85.
[31] Zabisky RCM, Chan W-M, Gloor PE, Hamielec AE. Polymer 1992;33(11):2243–62.
[32] gPROMS advanced user guide. Process System Enterprise Ltd.; 2004.